Bio-Enabled Synthesis of Metamaterials

Christopher C. DuFort and Bogdan Dragnea

Department of Chemistry, Indiana University, Bloomington, Indiana 47405; email: cdufort@indiana.edu, dragnea@indiana.edu

Annu. Rev. Phys. Chem. 2010. 61:323–44

First published online as a Review in Advance on January 4, 2010

The *Annual Review of Physical Chemistry* is online at physchem.annualreviews.org

This article's doi: 10.1146/annurev.physchem.012809.103300

0066-426X/10/0505-0323$20.00

Key Words

nanophotonics, virus, biomaterials, plasmonics

Abstract

Biological systems offer more than an inspiration for the spontaneous hierarchical organization of matter at length scales between 1 and 1000 nm. They also provide useful principles and molecular building blocks that have recently emerged with the proven ability to generate extended three-dimensional structures of hybrid biotic/abiotic components arranged with molecular precision. These principles and tools draw from the methods of molecular biology and modern biochemistry and are expected to provide unmatched flexibility in building supramolecular architectures, notably structures made of artificial atoms whose coupled responses to electromagnetic or elastic excitations have been predicted to yield astonishing properties unparalleled by any conventional materials. To illustrate the potential of merging bio-enabled organization with metamaterials synthesis, we provide here a succinct overview of the architectural constraints leading to metamaterial behavior together with examples of biological material assembly that are particularly promising to comply with these constraints.

INTRODUCTION

Metamaterials have physical properties determined by their organized structure rather than inherited directly from the material properties of individual subunits (1). In metamaterials, artificially structured mesoscopic inclusions usually replace the atoms and molecules of conventional materials (2). Properties unlike those of any known conventional material can be achieved this way. For example, elastic metamaterials can exhibit a negative effective Young modulus, i.e., an increasing volume under a compressive triaxial stress (3, 4). The electromagnetic counterpart of elastic metamaterials is represented by optical metamaterials with a negative index of refraction (5). In this case, for instance, composite architectures have been proposed that exhibit magnetic properties despite the nonmagnetic character of their constituents (6). As a result of its technological promise for optical super-resolution and other imaging applications, the field of optical metamaterials is currently experiencing explosive growth (7).

As with conventional materials, properties of metamaterials can be described by a small set of effective material constants, provided the operating wavelength, be it elastic or electromagnetic, is much larger than the spatial period characterizing the particular arrangement of mesoscopic subunits. The presence of defects in the periodic arrangement changes these properties and interferes with the wave propagation. Fabrication methods are required to achieve three-dimensional (3D) lattices with accuracies in the placement of the building blocks that are better than a fraction of the wavelength. For negative index of refraction metamaterials, for example, the building blocks have to exhibit an optical resonance at the excitation wavelength. One way to achieve this is by using metal inclusions that support surface plasmon resonances. Plasmons are collective oscillations of the valence electrons that have close to X-ray wavelengths at optical frequencies. Therefore, with a wavelength that is significantly shorter than the vacuum wavelength of the light, the requirement for accurate positioning of a plasmonic lattice element becomes even more stringent.

Because of this requirement, the current challenge for optical metamaterials is to devise methodologies that are able to provide nanoscopic accuracy in the positioning of the building blocks and 3D control over the symmetry of the architecture. In particular, for metallodielectric metamaterials to be useful in the visible range of the electromagnetic spectrum, extended 3D structures with lattice constants between 10 and 100 nm are required. Metamaterials with these constraints are difficult to synthesize with current microlithographic technologies.

The main aim of this article is to present bio-enabled self-organization as a possible means of combining the natural characteristics of self-assembling biomolecules and the physical properties of inorganic nanoparticles. This is done with the goal of obtaining metamaterials exhibiting novel optical properties. We are motivated in this endeavor by the idea that a bio-enabled approach could bring features unavailable in conventional materials fabrication, such as (*a*) self-recognition and defect rejection upon self-assembly, (*b*) the possibility of lattice engineering using established molecular biology methods (e.g., mutagenesis), (*c*) real-time switching of the lattice parameter using conformational changes in response to environmental cues, and (*d*) environmentally benign fabrication processes.

The incredible diversity and complexity of biological systems result in large part from their ability to derive functional attributes from their organized structure while using a relatively small set of building blocks. In this sense, metamaterial design aspires toward similar goals, which makes the idea of bio-enabled fabrication a natural choice. However, the ability to program structures into three dimensions with precise control of nanomorphology is likely to have applications that extend beyond metamaterials and may include solar energy harvesting, molecular separation, sensors, energy storage, pharmaceutical agent delivery, and nanoreactors.

From the three general strategies for the creation of new materials (biomimicry, bioinspiration, and bioderivation), we mostly deal herein with bioderivation, which involves the use of an existing biomaterial (protein, DNA) in concert with an abiotic material to create a hybrid. Examples include 3D DNA-assisted crystallization of metal nanoparticles, virus-surface scaffolds for nanoparticle networks, optical coupling of virus-encapsulated gold nanoparticles, and energy transfer along engineered helically symmetric virus scaffolds.

SPATIAL SCALES IN METALLODIELECTRIC METAMATERIALS

Metallodielectric nanostructures are host to a number of fundamentally interesting and technologically important phenomena. These include the facilitation of large electromagnetic enhancements for nanoparticle-enhanced spectroscopies (8), light confinement for subdiffraction imaging (9), exotic coatings (10), and light-directed crystallization and phase transitions (11).

Metallodielectric materials discussed here are made with components possessing dimensions much smaller than the wavelength of light. Similar to conventional materials, the electromagnetic response is completely described by two parameters: the bulk dielectric function, ε, and the magnetic permeability, μ. In addition, we are considering those metallodielectric materials that rely on metal inclusions that support plasmons because the dielectric function rapidly changes from positive to negative in the vicinity of the plasmon resonance. Thus, control over the plasmon resonance enables control over the sign of the dielectric function.

Plasmon resonance control can be exerted via the lattice parameter, shape, and composition of the metallic subunit (12). In many cases, the sensitivity of the plasmon resonance to these parameters is exquisite, a feature that represents the basic premise for plasmonic nanostructure applications in biosensing (13). Studies of the plasmon resonance dependency on these parameters abound in the literature, and a number of comprehensive reviews exist (14). In the following we consider three canonical systems of increasing complexity that help benchmark and illustrate the circumstances in which rigorous positioning control of components may be needed. We are thus interested in establishing the level of fabrication tolerance required to obtain 3D metamaterials with properties determined by the coupling of their optically active components. This is a departure point for the second part of the review, which is dedicated to bio-enabled bottom-up approaches of 3D metamaterial fabrication that could potentially perform within the desired bounds.

The first system discussed is the spherical gold nanoparticle, one of the most basic plasmonic nanostructures (15). Its optical properties in the visible and near infrared are dominated by the collective response of the conduction electrons to the electric field of light, which gives rise to a specific resonance band (**Figure 1**).

For small gold nanoparticles (below ~6 nm), the surface plasmon resonance peak wavelength varies with the diameter of the particle:

$$\frac{\Delta\lambda_{\text{peak}}(\text{nm})}{\Delta\phi_{\text{particle}}(\text{nm})} \approx 10.$$

The origin of this dependency arises from the particle size being comparable to the mean free path of conduction electrons, which increases the damping rate and changes the permittivity with respect to its bulk value (16).

Between ~6 and 30 nm, the position of the plasmon peak is insensitive to changes in the particle diameter. In this regime, permittivity assumes that the bulk value and the external electric field can be considered constant across the entire diameter of the sphere with no retardation effects. The plasmon oscillation corresponds to a dipole mode. As the particle size increases beyond ~40 nm, the extinction cross section is determined by the superposition of dipolar, quadrupolar,

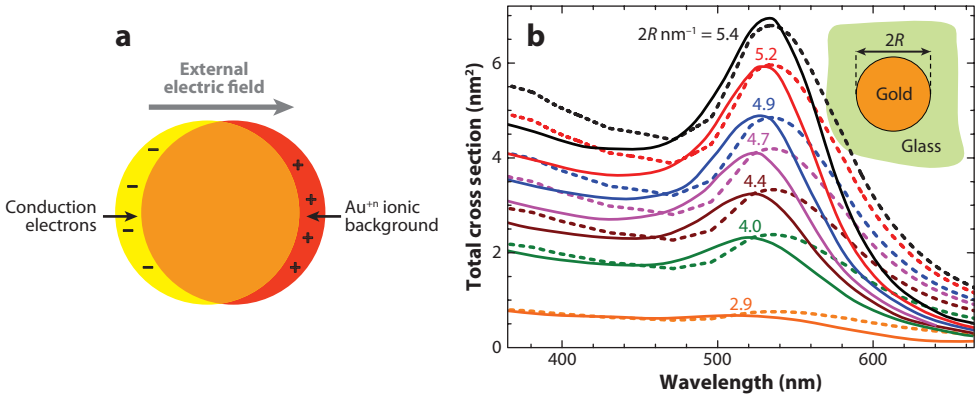

Figure 1

(*a*) Schematic of a dipolar plasmon oscillation in a gold nanoparticle. (*b*) Total cross section (extinction) by gold nanoparticles of different sizes, which are much smaller than the wavelength of light. Experiment (*solid lines*) is compared with theory based upon finite-size corrected permittivity values (*dashed lines*). Figure adapted from Reference 15, with permission from The Royal Society of Chemistry.

and higher-order mode contributions, and the polarizability is a sensitive function of the size parameter ($2\pi R/\lambda$) (**Figure 2**).

Plasmonic nanoparticle pairs known as dimers embody another simple system. These dimers have been studied most extensively in relation to their promise in generating intense near-field intensities for applications in surface-enhanced spectroscopies and for developing an understanding of coupled plasmons (17).

Nordlander et al. (18) have described the optical near-field coupling between pairs of spherical particles in terms of the hybridization of single-particle plasmonic modes, a conceptual picture

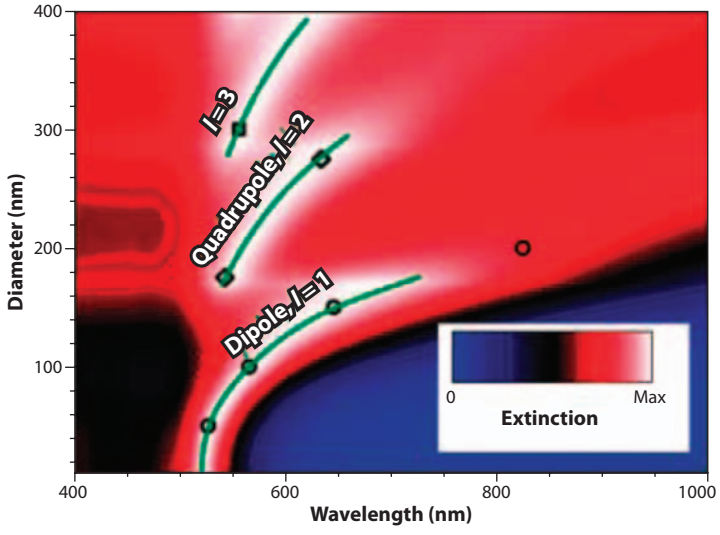

Figure 2

Evolution of the extinction spectra for nanoparticle sizes larger than 10 nm. As the particle size increases, the extinction maxima red-shift, and multipolar plasmon oscillations emerge. Figure adapted from Reference 15, with permission from The Royal Society of Chemistry.

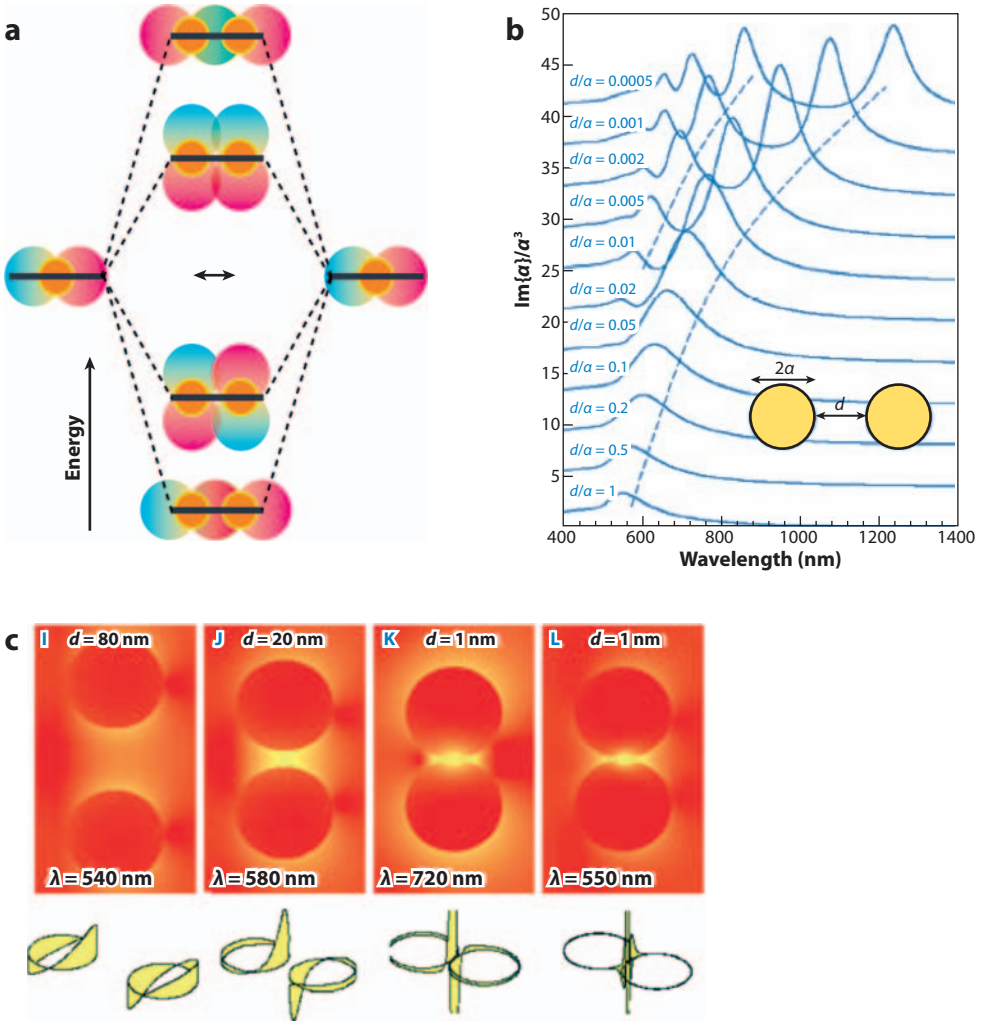

Figure 3

(*a*) Hybridization model describing the interactions between two closely placed spherical particles supporting in-phase and out-of-phase plasmon wave functions. (*b*) The imaginary part of the polarization of a pair of nanoparticles (radius $a = 30$ nm) as a function of the interparticle distance. The applied electric field was polarized along the interparticle axis. (*c*) Near-field maps of the squared electric field around nanoparticles and the corresponding induced surface charge shown as a 3D plot (*below*). Figure adapted from Reference 17, with permission from the Optical Society of America.

borrowing from molecular orbital theory (**Figure 3*a***). The degeneracy of the single-particle mode is lifted by coupling, and new modes appear in the extinction spectrum. Romero et al. have theoretically studied the polarizability of the dimer formed by two spherical gold particles ($a = 60$ nm) for different distances, d, between their surfaces. They found that the resonances shift with the interparticle distance approximately as $d^{1/2}$ and the shift starts as soon as $d \approx a$.

As the particle separation is reduced further, the surface plasmon modes red-shift. Initially, the far-field response weakens because the effective dipole of the coupled dimer is reduced. However, for smaller separations there is a strong buildup of charge at the gap, which is responsible for the

enhancement of the near fields in this region, and the far-field scattering begins to increase again (17, 19). When two particles are near touching ($d/a \approx 0.001$–0.01), there is a dramatic enhancement of the induced electric field at the point of maximum proximity. It is here that modes corresponding to higher multipoles appear and disappear, and a singular transition occurs when the particles touch (17). This qualitatively different near-touching regime would therefore correspond to distances of ~1 nm between nanoparticles of several hundreds of nanometers in diameter. It is this regime that has been invoked to explain the extraordinary field enhancements responsible for single-molecule surface-enhanced Raman scattering from metallic nanoparticle substrates (20). Thus, the extreme modification of the overall optical response due to minute changes in relative spacing opens up new approaches for ultrasensitive molecular sensing and spectroscopy.

The mixing and splitting of individual particle modes observed for nanoparticle dimers lead to the formation of a band structure when metallic nanoparticles are arranged periodically in extended 2D and 3D lattices (21, 22). When the distance between spheres is much smaller than the wavelength of light, the optical properties of such a composite medium can be described by an effective dielectric function, ε_{eff}. In the case of 3D metallodielectric materials, the important structural parameter is f, the fractional volume occupied by the metal spheres. This is also known as the filling factor, the 3D counterpart to d/a that is useful for particle dimers. In the approximation of only dipolar contributions from the metal particles, the effective-medium theory yields the Maxwell Garnett expression:

$$\varepsilon_{eff} = \varepsilon_m \frac{1 + f \cdot \frac{2(\varepsilon_s - \varepsilon_m)}{\varepsilon_s + 2\varepsilon_m}}{1 - f \cdot \frac{\varepsilon_s - \varepsilon_m}{\varepsilon_s + 2\varepsilon_m}},$$

where ε_m and ε_s are the dielectric constants for the homogeneous embedding medium and the spheres, respectively. The Maxwell Garnett equation is accurate at small values of f and low frequencies. It predicts a single plasmon for the composite medium at a frequency that is a function of f and particle radius (**Figure 4**) (22). However, when f becomes large (i.e., metal particles are close together), the effective-medium approach, as represented by the Maxwell Garnett equation,

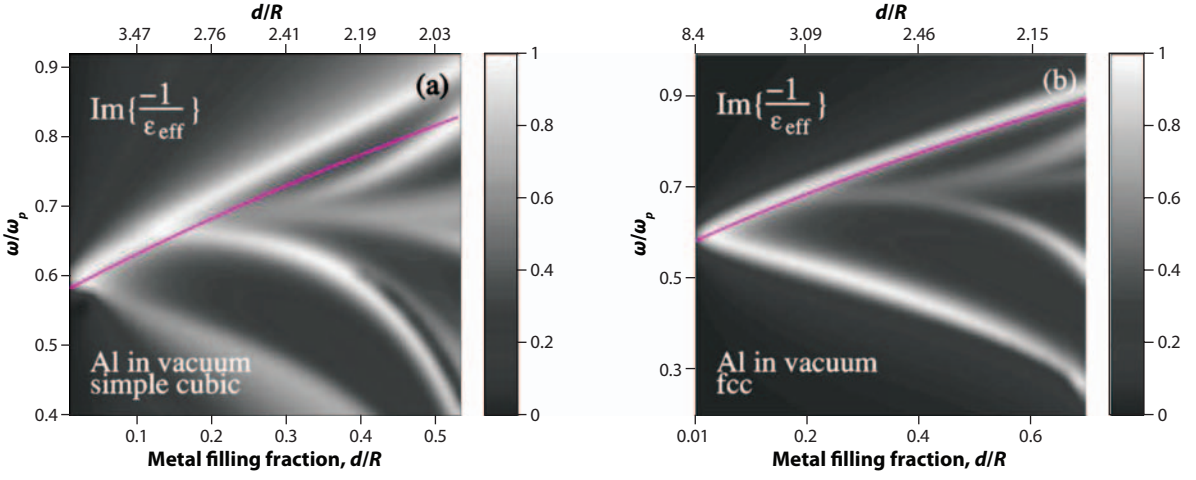

Figure 4

(*Solid curve*) The Maxwell Garnett plasmon for a 3D metallodielectric medium characterized by dipolar interactions only. (*Density plot*) Exact solutions of Maxwell's equations showing a band structure determined by multipolar term contributions and local order. Brighter regions correspond to low absorption. Here R is the radius of the particles, and d is the center-to-center distance in a cubic lattice. Figure adapted from Reference 22, with permission from the American Physical Society.

deviates considerably from exact treatments of Maxwell's equations (21). Moreover, the Maxwell Garnett formula does not contain an explicit local order contribution; the dielectric constant is the same for an ordered or a disordered medium.

However, the most interesting properties from a technological point of view, such as regions of frequency over which light cannot exist within a 3D crystal, occur for large metal filling fractions *f* (**Figure 4**). In this case, the particles have to be separated by distances equal to a fraction of the particle radius. For example, in the case of 50-nm particles, an ~5-nm dielectric spacer would be required, which implies a tighter control on the size and location of the components than most top-down fabrication methods can currently provide.

Understanding the effect of disorder on the effective-medium permittivity is important because sub-10-nm positioning accuracy and monodispersity in the size of artificial atoms remain challenging goals for present manufacturing techniques. Yannopapas (23) studied the issue of disorder in a metallodielectric material, showing that the effective permittivity of a partially disordered metallodielectric array is always greater than that of a corresponding perfect crystal for the same filling fraction, *f*. Another expected effect of disorder would be a broadening of the spectral features shown in **Figure 4**.

Finally, the important role played by the interparticle distance in metalodielectric metamaterials is not exclusive to metal particle coupling. The lifetime of an excited fluorophore depends not only on its molecular structure, but also on its environment. For example, close to a metal surface, the fluorescent emission exhibits either enhancement or quenching, depending on the fluorophore-metal surface distance. The way in which the fluorescence rate varies with respect to its nonperturbed value is determined by the balance between the near-field enhancement in the vicinity of a metal surface (discussed above) and the quantum yield. The latter depends on the ratio between the radiative and nonradiative excitation lifetimes, which are functions of fluorophore-metal surface distance, molecular transition dipole orientation, and plasmon frequency. Anger et al. (24) have studied the fluorescence rate of a single molecule as a function of its distance to a laser-irradiated gold nanoparticle (**Figure 5**). Enhancement at distances greater than 5 nm was observed, while quenching of fluorescence occurred for shorter distances (**Figure 5*c***). The theoretical analysis based on the dipole approximation described the enhancement factor as dominating at large separations reasonably well. However, the dipole approximation failed to predict the decrease in quantum yield observed for distances below 5 nm. To reach agreement, higher multipole modes were needed for a more accurate description of the nonradiative rate (24). Dulkeith et al. (25) have shown that, at distances of ~1 nm, the quenching results not only from an increased nonradiative rate, but also from a significant decrease in the fluorophore radiative rate.

A related example of the elegant control of photophysical processes on the nanometer scale has been demonstrated by Ringler et al. (26), who embedded fluorophores in nanoparticle dimer resonators by means of biomolecular linkers (**Figure 6**). In this case, the coupling between molecular transitions and plasmonic resonances of the particle dimer provides an additional control parameter. This influences not only the fluorescence emission rate, but also the shape of its spectrum. The nanoparticle dimer resonator selectively enhances the probability of resonant transitions. The use of biomolecular linkers based on antibody/antigen interactions provides interparticle distances between 1.2 and 13.3 nm, so a wide range of resonances can be realized.

In conclusion, in the case of both passive (transmission/reflection) and active (luminescent) metallodielectric materials, technologies enabling the fabrication of structures with components spaced at the 1–10 nm scale should provide control of a host of phenomena responsible for exquisite spectral properties at visible wavelengths.

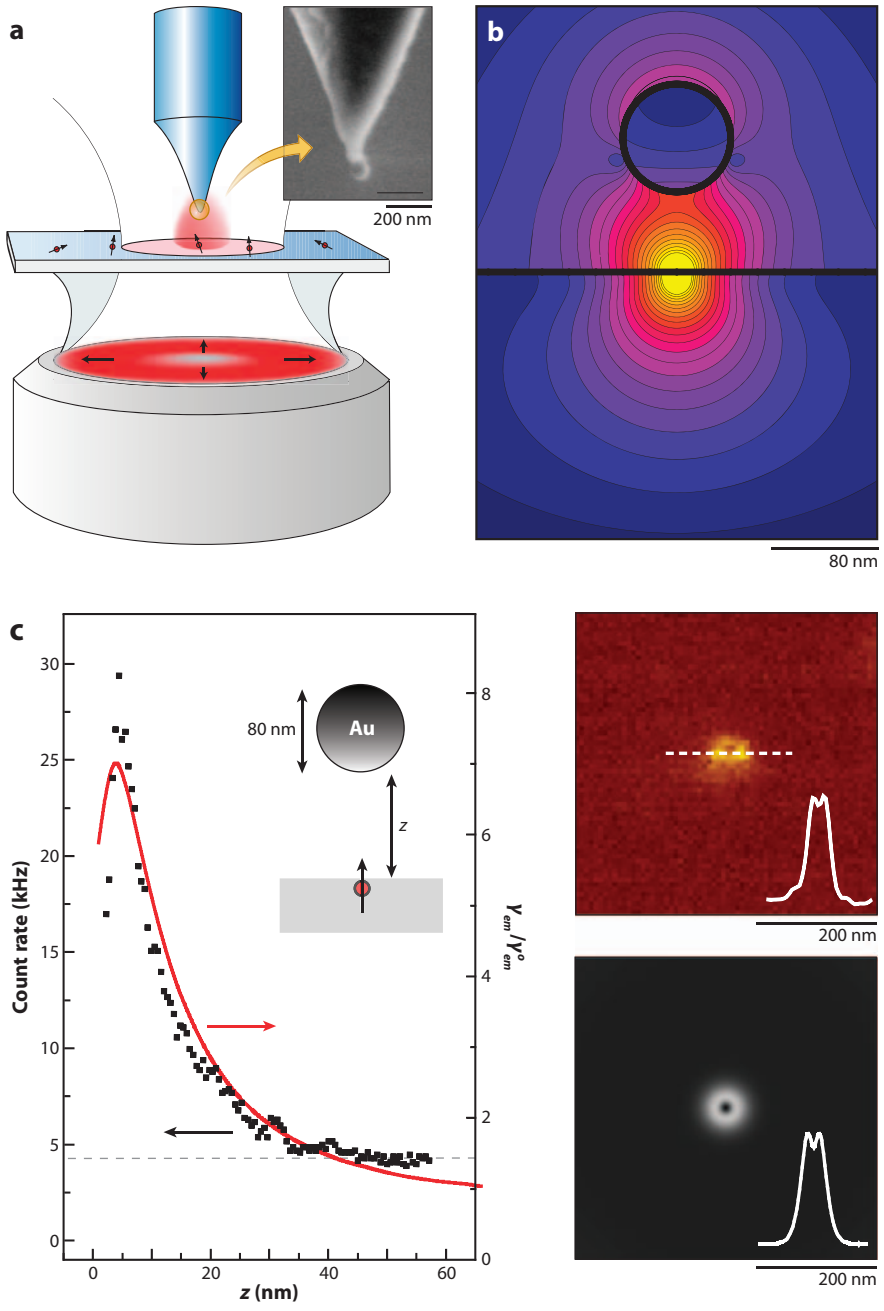

Figure 5

(*a*) Experimental setup for measuring the fluorescence of a single molecule as a function of distance to a metal nanoparticle. (*b*) Calculated field intensity distribution. (*c*) Fluorescence rate as a function of particle-surface distance (the *red curve* represents theory, whereas *black dots* represent experiment). Figure adapted from Reference 24, with permission from the American Physical Society.

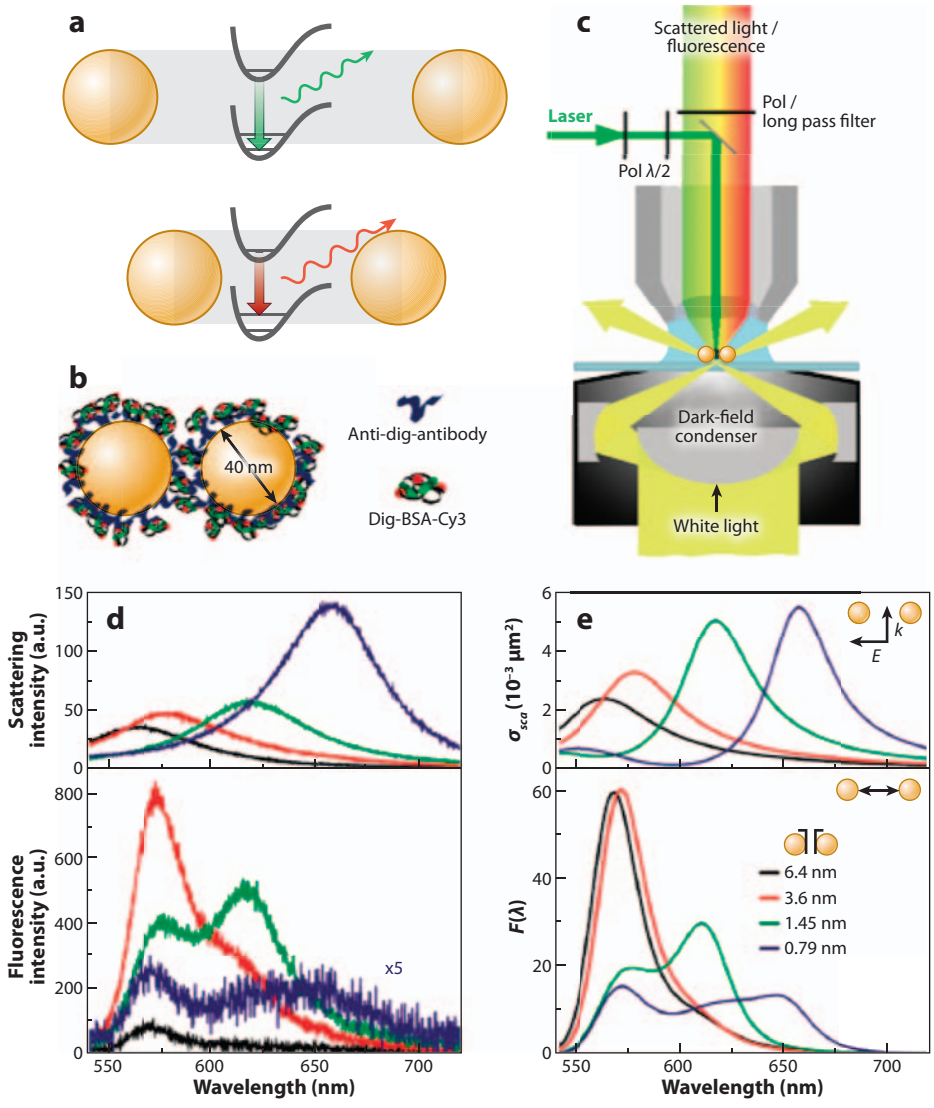

Figure 6

(*a*) Radiative transitions to different ground-state sublevels are enhanced if these sublevels correspond to a high density of near-field modes. (*b*) Schematic of plasmonic particle dimer resonators held together by biomolecular interactions. (*c*) Experimental setup. (*d*) Experimental scattering and fluorescence spectra of particle dimers. (*e*) Theoretical scattering cross section and fluorescence emission as a function of wavelength. Figure adapted from Reference 26, with permission from the American Physical Society.

THE BIOMOLECULAR TOOLBOX

Bottom-up techniques, such as self-assembly and directed assembly, are examples of alternative fabrication methods to top-down techniques. Besides operating at the correct spatial scale, they offer potential advantages in cost, sample size, and fabrication speed.

Although countless examples of self-assembled systems can be found in living matter, nonbiological approaches have been the first to deliver a number of notable examples of systems exhibiting

metamaterial properties. Thus, the integration of colloidal particle self-assembly and plasmonics is well underway at the level of basic science (12). The achievements in this area mainly result from advances in colloidal particle chemistry, including low size polydispersity, capping ligand chemistry, morphology, and composition control.

Figure 7 presents an example of the guided organization of silver nanoparticles into 3D structures of different crystallographic symmetry (27). Colloidal dispersions of polyhedral silver nanoparticles adopted ordered structures under slow sedimentation and subsequent solvent evaporation. The order in this case comes from steric repulsion between individual nanocrystals under the gravitational constraint. The dimensions of dried assemblies scale up to a few millimeters. As predicted in the theoretical work outlined in the first section, optical passbands occur, which are a function of the metal volume fraction (**Figure 7*b***). Changing the shape of the silver subunit from octahedral to cubic nanocrystals results in different lattice structures (27).

One challenge inherent to colloidal assemblies for optical metamaterial applications remains the variability of the subunit, which may come from the growth of the metal particle itself or from the bulky capping polymer ligand, which makes for a heterogeneous subunit interface at the molecular scale. For colloidal particles with diameters ranging between 2 and 200 nm, the relative size variance is a few percent or more. Thus, in a chain of particles, the root-mean-square value of the deviation in the position of the n-th particle from its expected value, $n \cdot a$ (where a is the average diameter, same as the lattice constant), is $\sigma \cdot n^{1/2}$, where σ is the standard deviation in the particle diameter (**Figure 8*a***). Hence, long-range order may be considered practically destroyed in approximately $(4\ \sigma^2)^{-1}$ cells. The long-range order can be restored if the particles are placed in cages that have essentially zero size variability (**Figure 8*b***). In this case, the deviation of the n-th particle in the chain from its position in a perfect lattice does not depend on n, but solely on the positioning tolerance within the cage.

Examples of single-size mesoscopic molecular cages abound in nature: icosahedral virus capsids, ferritin protein cages, clathrin cages, and protein vaults. Questions that come to mind are then, (*a*) What happens with the band structure if long-range order is restored this way? (*b*) Is it possible to encapsulate nanoparticles in the natural cavities of these biomolecular cages without significantly perturbing their molecular structure, and then let the cages assemble in the way molecular crystals grow, thus producing a hierarchical structure? We deal briefly with the first question in the following, whereas the second is the object of a more detailed discussion below.

The classical Kronig-Penney model of the electronic wave function propagation in a 1D square-well periodic potential, for which the Schrödinger equation can be solved analytically, has been used by Makinson & Roberts (28) to study the effect of short-range and long-range order on the electronic band structure of a linear chain of δ potentials. This model can be adapted to our case for a qualitative discussion, as the Schrödinger equation and the electromagnetic wave equation for an inhomogeneous medium are formally equivalent (29).

Our purpose is to compare the energy band structure of the linear chain in **Figure 8*a*** with the one in **Figure 8*b***. In the original Kronig-Penney model, the positions of the potential wells are distributed in a perfect lattice. The potential strength (describing the inhomogeneous intrusions in our case) is the same for each cell. The number of states per unit length N, as a function of energy ν, is plotted in **Figure 8*c***. A horizontal portion of a curve for $N(\nu)$ signifies an absence of states in that range of ν, i.e., an energy gap.

For the chain in **Figure 8*a***, each potential well is randomly displaced from the corresponding ordered lattice point according to a normal probability distribution. The interaction between the propagating wave and the inhomogeneous inclusion (particle) is also modeled by random values distributed around an average potential strength. Relative standard deviations used in calculations are 10% for both position and potential. For the chain in **Figure 8*b***, the randomness in position is

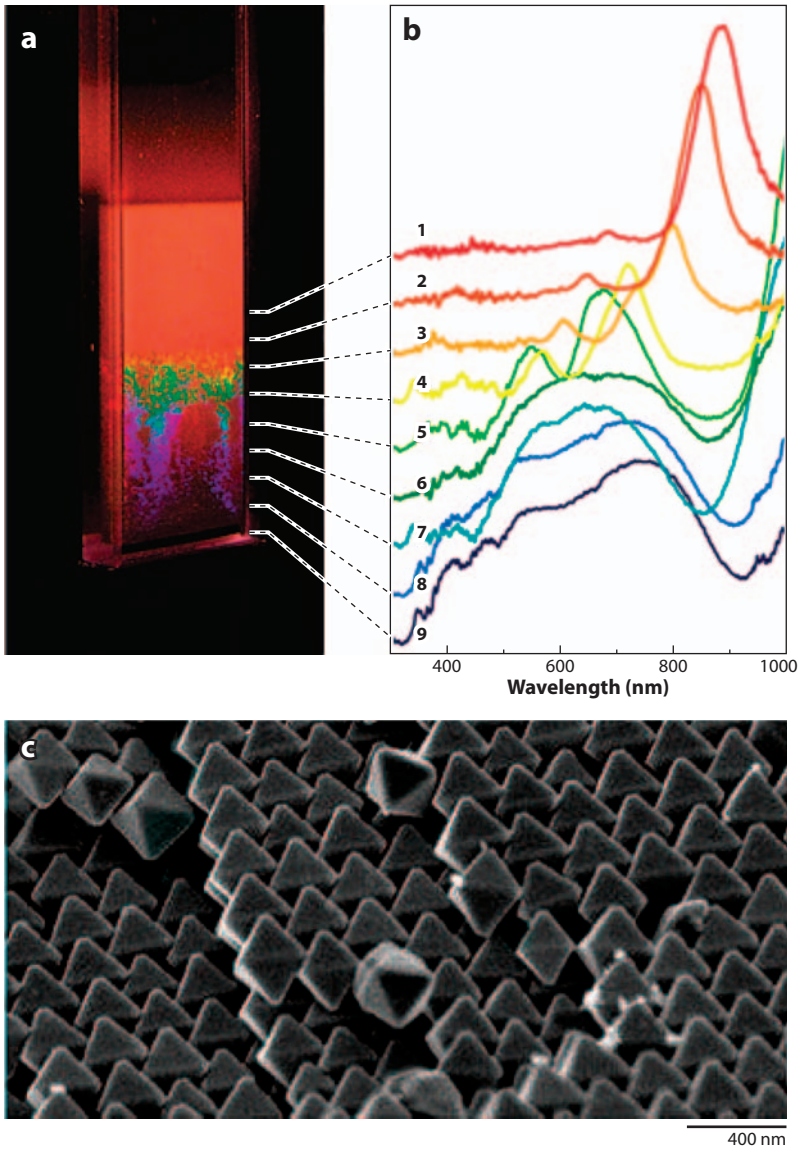

Figure 7

(*a*) Sedimentation-assisted assembly of colloidal crystals of Ag nanoparticles (~150 nm in size). (*b*) Specular reflectance spectra collected from different heights in the cuvette (different heights correspond to different filling factors). (*c*) Scanning electron micrograph of the surface of a cleaved crystal. Figure adapted from Reference 27, with permission from the American Chemical Society.

considered absent, but the one in potential strength is present. For the chain in **Figure 8*a***, they are both present. The results show that, whereas a completely ordered system of identical potential wells presents a well-defined gap, the gap closes to approximately half its unperturbed value for the case of regularly placed, but randomly, deep potential wells. This then vanishes altogether when random deviations in the position of embedded inhomogeneities are added.

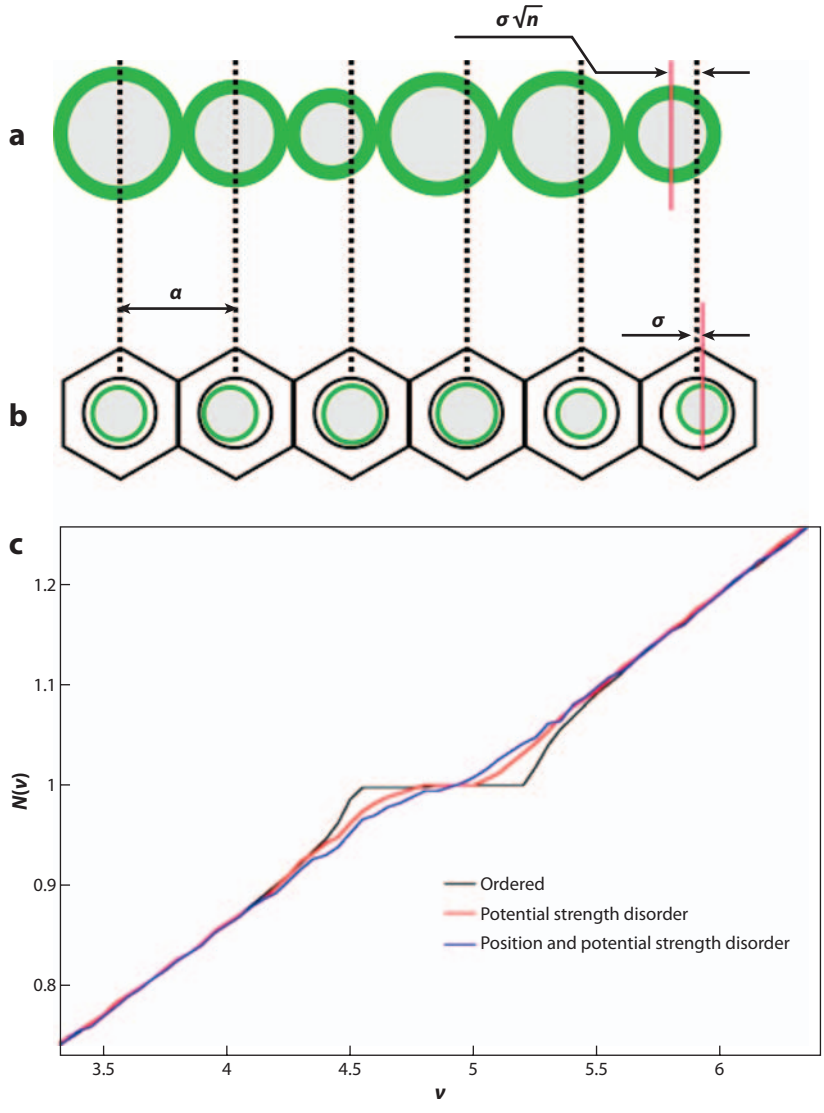

Figure 8

(*a*) A colloidal linear chain exhibiting loss of long-range order. (*b*) Linear chain of caged colloidal particles with only local disorder. (*c*) The number of states per unit length as a function of energy for the ordered model of Kronig and Penney, for a linear chain with disorder in the potential strength and a linear chain with disorder in both position and potential strength.

In conclusion, the use of molecular constructs to remove the long-range disorder is expected to decrease spectral broadening and sharpen the forbidden band edges in plasmonic metamaterials, which have a direct impact both on applications and on benchmarking for theory development.

Let us now turn our attention toward the second question, What types of molecular constructs exist that can provide us with tools for organizing nonbiological matter? Natural biological organization employs three basic macromolecular structural building blocks: lipids, polysaccharides, and proteins. Among them, proteins have the greatest structural diversity and multiple levels of

organization, represented by amino acid sequence, helices and strands, structural motifs, globular domains, protomers, and oligomers. Unlike lipids, for example, which organize forming interfacial regions of different shapes and sizes due to their low aqueous solubility, there are numerous examples of protein assemblies that exhibit high-order symmetry and well-defined size. Symmetry often confers stability on the molecular system and results in economical usage of basic components and information storage (by nucleic acids). The resulting functional complexes usually represent far more than the sum of their parts.

Whereas nucleic acids are macromolecules with the role of ensuring information storage and transmission in nature, their robust self-assembly properties, in particular the rigid double-helix structure and the base pairing of DNA, enable recognition and high binding selectivity. One advantage of DNA-based approaches is the ability to use automated polymerase chain reaction to synthesize large quantities of any sequence with control over the length and functionality. The ability to create DNA strands with any desired sequence of bases has led to the rational design of various DNA-based nanostructures (30, 31).

The feasibility of utilizing DNA oligonucleotides as mediators for the guided assembly of nanoparticles was first addressed over 10 years ago in the pioneering work of Mirkin and colleagues (32) and Alivisatos and colleagues (33). However, the creation of a 3D hierarchical assembly of gold nanoparticles in a crystalline lattice has remained a challenge, as many of the early attempts tended to result in amorphous aggregates.

Nykypanchuk et al. (34) devised a system that uses two types of single-stranded DNA. One strand contains complementary base pairs exhibiting an attractive force between particles, and another noncomplementary type provides a repulsive interaction. Control over the rate of assembly, morphology, and aggregate growth can be achieved through the tuning of the ratio of complementary to noncomplementary DNA. In their approach, ~11-nm gold nanoparticles are capped with complementary DNA molecules and allowed to self-assemble under varying temperatures and length of DNA linker molecules. Two conditions produced crystalline structures with long-range order, those with the relatively long and flexible 35- and 50-base length linkers.

The crystallite size was estimated from the small-angle X-ray scattering correlation length at ~500 nm. The filling factor of the DNA/gold nanoparticle materials in these examples was low, between 2% and 4%, with the DNA occupying 4%–5% and the remaining being filled with solvent. Therefore, it is unlikely that such a material will exhibit plasmonic properties characteristic for strongly coupled metal particle systems.

For stronger coupling effects, shorter spacers are required. However, the shorter rigid spacers typically produce amorphous aggregates. This likely results from the spatial flexibility afforded by the longer strands. When heated to near the melting temperature, the particles are able to reorient themselves into a configuration consistent with a local energy minimum, resulting in a crystalline lattice. One of the most important lessons from this work is that there is an intimate relationship between the repulsive and attractive forces in DNA-linked nanoparticle aggregates, which can be tailored for the synthesis of highly ordered structures.

In the above example, the molecular scaffold is likely to be in a partially disordered state, comparable with that of a polyelectrolyte brush, whereas the metal cores are organized in an ordered lattice at a mesoscopic scale. However, 3D DNA-based structures ordered at a molecular scale can be obtained from branched DNA subunits. This approach significantly expands the structural lattice options with respect to naturally occurring linear DNA. A few examples include cubes (35), tetrahedra (30, 36–37), octahedra cages (39, 40), dodecahedra (30, 41), and buckyballs (42). However, whereas short DNA subunits often provide sufficient rigidity for building hierarchical 3D arrays, DNA-based scaffolds are usually open and flexible at the mesoscale. An alternative approach is to use the other major class of bioderived fabrication materials: proteins.

Unlike DNA, whose double-helical structure comprising a set of nucleotides attached to a sugar-phosphate backbone is understood in detail, proteins are linear polymers of L-amino acids organized in a hierarchical way. The multiple levels of protein organization make the problem of protein folding and protein interactions more difficult to predict and engineer. Despite this difficulty, there are a few examples of proteins optimized by evolution to perform the task of guiding abiotic material organization. For example, the supermechanics of the glass skeleton of the deep-sea sponge *Euplectella* is the result of seven hierarchical levels (43) in which proteins not only guide the growth of the inorganic material (silica), but also play an active role in its mechanical performance, such as preventing the propagation of cracks.

Other proteins are adept at self-assembly and encapsulation of selected molecular cargoes. One example is the coat proteins of small spherical viruses, which predominantly exhibit icosahedral symmetry. Such a virus is built as a quasi-spherical protein container encapsulating the virus genome in its internal cavity. According to Caspar & Klug's (44) quasi-equivalence theory, the protein shell, also termed the capsid, is made of pentamer and hexamer subunits, the number and arrangement of which are determined by a triangulation number, termed the T number: $T = h^2 + k^2 + hk$, where h and k are nonnegative integers and T is an integer value (e.g., 1, 3, 4, 7, 12, 13). For an icosahedral shell (5:3:2 symmetry), there are 12 pentamers and 10 $(T - 1)$ hexamers (45).

Besides virus capsids, other protein assemblies exhibit high levels of symmetric organization, for example, the octahedral 4:3:2 symmetry found in ferritin. From a materials perspective, this high degree of symmetry is important for a number of reasons. First, viruses have monodisperse structures with intrinsic polyvalency of chemically addressable sites on the capsid surface (46), allowing inorganic nanomaterials to be attached at well-defined locations in a symmetric arrangement. Second, they spontaneously self-assemble, and the result of the self-assembly process depends on the environmental conditions or the genetically engineered state of the protein (47). Third, all the interfaces of the capsid offer a environment for controlled growth or chemical manipulation involving abiotic materials (48, 49) or for encapsulation by self-assembly (50). Fourth, viral and nonviral self-assembled protein cages occur in a variety of shapes (not only icosahedral) and sizes. These range from the 18-nm ferritin octahedral cage to the 500-nm giant of an icosahedral virus, the mimivirus (51) (**Figure 9)**. This variety provides a library of platforms for tailored applications, including the hierarchical assembly of metallodielectric materials.

In the following, we discuss two examples of gold nanoparticle virus-based metallodielectric materials. The first concerns the utilization of the *cowpea mosaic virus* as a scaffold for external 3D patterning with a network of gold nanoparticles arranged with a resolution of 28 Å (52–54). The intact *cowpea mosaic virus* capsid has an average diameter of 28.4 nm and is in a class of small icosahedral plant viruses. It comprises 60 copies of an identical protein subunit. Different crystal forms of the virus can be readily produced under well-defined conditions. Because of the repeating nature of the capsid, any modification made to any subunit is copied 60 times and is incorporated into 60 distinct locations of the virus capsid upon self-assembly of the protein subunits (55). Utilizing this approach, Johnson and colleagues (52, 54) devised a method to modify the coat proteins of CPMV to decorate the surface of intact capsids with gold nanoparticles at precisely controlled interparticle distances in three dimensions (**Figure 10**).

The work provides the first clear demonstration that accurate control of the interparticle spacing and 3D arrangement can be achieved in virus-based materials through both chemical and steric methods. However, the particle sizes were limited to gold nanoclusters, less than 2 nm diameter, and an estimated crystal filling factor below 1%. To obtain higher filling factors, a different approach allowing for the use of larger particles is necessary.

Although there are many methods for the 2D patterning of colloidal metal particles on surfaces (56–58), their arrangement in three dimensions with current fabrication methods remains

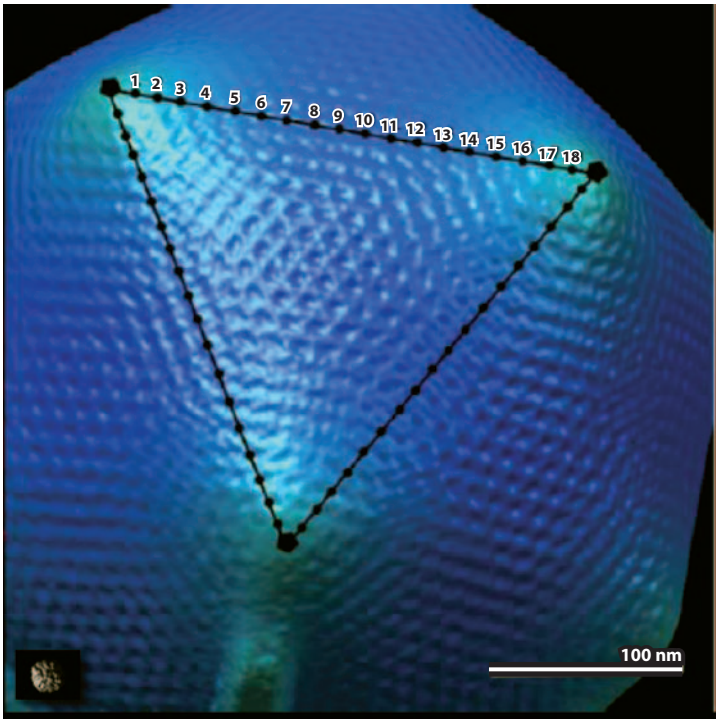

Figure 9

Image reconstruction from cryo-electron microscopy data of the largest known virus capsid, the mimivirus (51) together with a drawn-to-scale apoferritin protein cage (*inset;* Protein Data Bank).

a challenge. As discussed above, in any assembly technique that relies purely on the collective organization of colloids, long-range order is difficult to achieve because of the propensity for small variances in particle size to cause significant long-range defects. A molecular self-assembly approach is able to circumvent this problem owing to the inherent ability of colloids to self-check and regulate their structure with atomic level precision. This is because any small errors in the constituent protein subunits would disrupt the rigid spatial constraints of a virus capsid, making their incorporation into the final capsid unlikely. Utilizing a molecular mediated approach, such as crystallization, small variances in the size of colloidal particles are irrelevant.

One example is a virus capsid serving as a container for a colloidal particle. We have seen that very large (~500-nm) capsids exist, whereas the gyration radius of a capsid protein is 2 to 3 nm. Therefore, there is the potential for significant filling factors if the metallic particle resides inside the capsid cavity. As the particles are encapsidated within the virus shell, small variations in particle size no longer matter because small internal variations can be tolerated, as each virus capsid remains identical. Through this virus-based approach, it is possible to incorporate a variety of inorganic nanoparticles, such as quantum dots (59) and magnetic (60) and gold nanoparticles (61), into the interior of the capsid, or to even use them as nanoreactors (62, 63) for the seeding and subsequent growth of nanoparticles.

Here we discuss the generation of 3D hierarchical assemblies of gold nanoparticles through the crystallization of gold-core viruses. This type of assembly is predicated on the use of virus-like particles (VLPs). A VLP is one in which the viral genome has been removed and replaced with a functional moiety such as a nanoparticle while maintaining the native structure of the virus capsid.

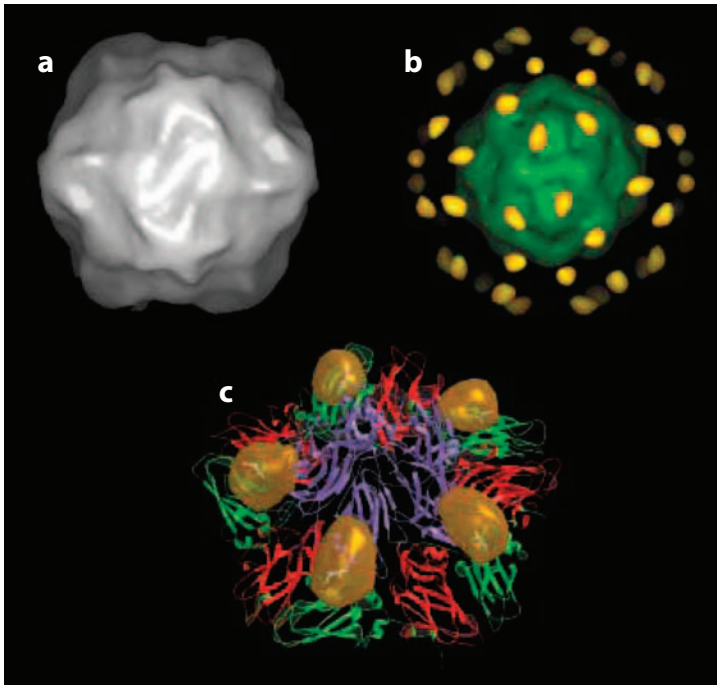

Figure 10

Cryo-electron microscopy image reconstruction of the 30-nm-diameter capsid of *cowpea mosaic virus* labeled with 1.4-nm gold clusters (*gray*, capsid protein; *green*, nucleic acid; and *yellow*, gold). Figure taken from Reference 52.

A well-studied virus in this application is the *brome mosaic virus* (BMV). It is a small icosahedral plant virus with a diameter of ∼280 Å that is composed of 180 identical proteins that self-assemble into pentamer and hexamer subunits that form a capsid exhibiting $T = 3$ symmetry. From its crystal structure, BMV is known to have an arginine-rich interior giving a positive charge to the inside of the shell. To mimic the viral RNA, gold nanoparticles with a diameter of ∼12 nm are functionalized with carboxylated polyethylene glycol. Through nonspecific electrostatic interactions, the virus protein subunits are able to self-assemble around the foreign core into an icosahedral structure with the same $T = 3$ symmetry as the native virus (64).

When exposed to the same crystallization conditions as native BMV, crystals of the same rhombohedral family, up to approximately 500 μm in length, form for VLPs and at any mixing ratio of BMV:VLP (50). The filling factor in this case is 8% with a rare occurrence of lattice defects, as can be seen from the atomic force micrograph of a crystal face shown in **Figure 11**. This is a common feature for some virus crystals (65), whereas others will allow for the incorporation of a wide range of unusual impurities, which is not possible for conventional crystals (66). The spectral properties of the gold-laden VLP crystals differ significantly from those of unorganized VLPs aggregating amorphously on a substrate or isolated in solution. As shown in **Figure 11**, a double feature in the absorption spectrum was observed, which is believed to provide evidence for multipolar coupling between adjacent gold nanoparticles (67).

In addition, preliminary X-ray diffraction data taken for the purpose of resolving the molecular structure of the composites exhibit diffraction peaks corresponding to 5-Å spatial resolution,

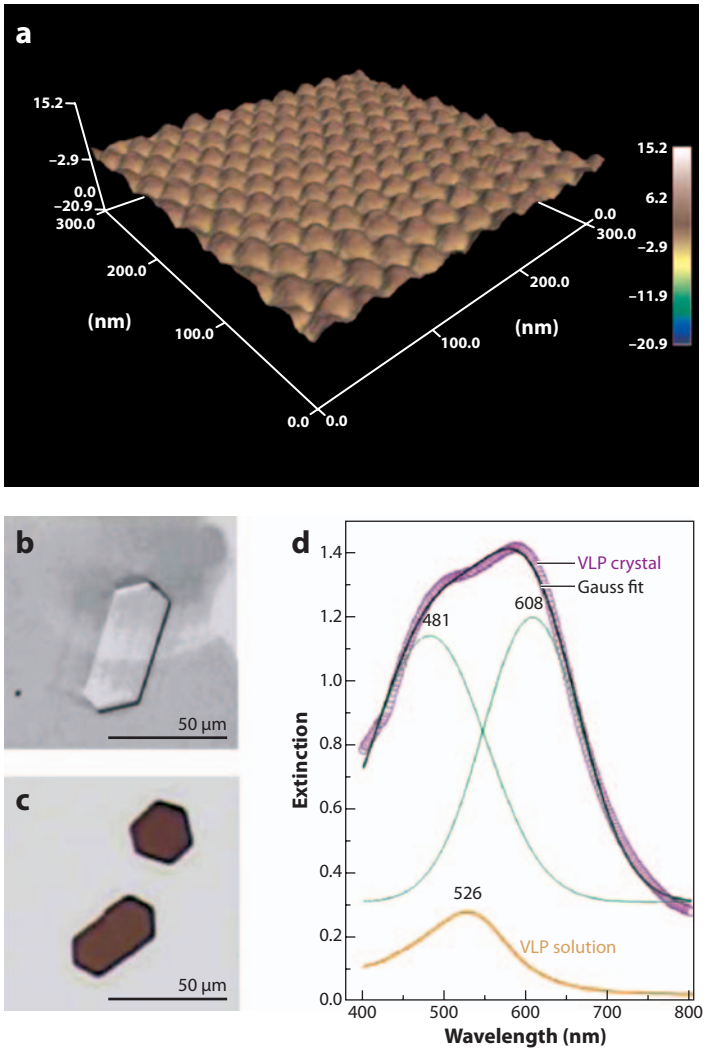

Figure 11

(*a*) The lattice constant of 27.8 ± 0.5 Å obtained for a *brome mosaic virus* (BMV) rhombohedral crystal by atomic force microscopy. Transmission optical images of a native BMV (*b*) and gold-core virus-like particle (VLP) crystal that has its deep red color due to the plasmon absorption band (*c*). The optical spectrum in panel *d* shows a double feature in the peak for a VLP crystal as compared to the well-known plasmon absorption band for a solution of well-separated 12-nm gold nanoparticles. Figure adapted from Reference 50, with permission from the National Academy of Sciences.

indicating that order is preserved down to the molecular scale despite the relatively massive metallic inclusions (68).

This feature of virus-based materials preserving the structural integrity, and thus symmetry of the molecular scaffold, may also become relevant for the field of energy harvesting. Although there is a diverse range of mechanisms used by light-harvesting biological organisms, one common feature to all of them is the requirement of an electron-transfer relay system. In such a system, a series of chromophores is arranged with nanometer precision in a 3D array, which enables

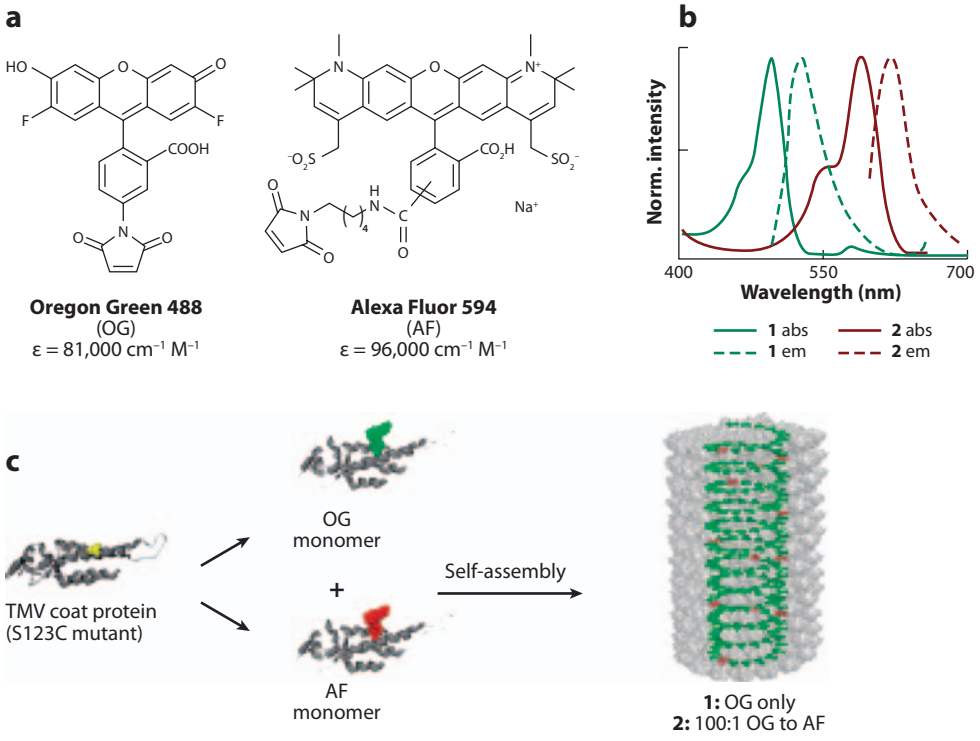

Figure 12

(*a*) An artificial light-harvesting structure created by the precise arrangement of the fluorescent molecules Oregon Green (OG) and Alexa Fluor (AF) to a virus scaffold. The absorption and emission spectra of the donor (OG) and acceptor (AF) chromophores are shown in panel *b*, and the molecules were attached at a ratio of 100:1, respectively. The chromophores were bound to the monomeric subunits of the *tobacco mosaic virus* (TMV) coat protein mutant S123C and self-assembled into rod-like structures with chromophores in a regularly patterned array. This was done for the donor molecule OG alone and for the donor-to-acceptor structure OG-AF at a ratio of 100:1 (*c*). Figure adapted from Reference 70, with permission from the American Chemical Society.

the efficient transport of energy through a series of Förster resonance energy transfer events (69).

For the demonstration of the feasibility of using viruses as scaffolds for the templating of regularly spaced chromophores to mimic a light-harvesting antenna, *tobacco mosaic virus* is an attractive candidate (69, 70). In its native form, it is a rod-like helical virus comprising 2130 identical protein subunits with an overall length of 300 nm and an outer diameter of 18 nm (**Figure 12**). A degree of structural diversity is also present, as the capsid protein subunits are known to self-assemble into a number of structures, including disks and rods, by making modifications to the pH and ionic strength of the assembly conditions.

To utilize the inherent ability of *tobacco mosaic virus* capsid proteins to form well-defined structures with atomic-level precision, Ma et al. (70) generated a monomeric S123C mutant. Upon self-assembly, the disk or rod structures contain repeating cysteine residues at precise positions that serve as binding sites for fluorescent molecules. The dyes chosen were Oregon Green 488 and Alexa Fluor 594 such that the spectral overlaps would enable donor-to-acceptor energy transfer via Förster resonance energy transfer, mimicking an energy relay system. The timescale of the

resulting energy transfer events was monitored by picosecond time-resolved fluorescence spectroscopy. The energy transfer occurred within 187 ps with an efficiency of ~36%, which is significantly slower than in natural photosynthetic systems, but compares well to other artificial systems, providing a useful benchmark for synthetic arrays based on self-assembling protein scaffolds. This is only one example of virus-based material that may become useful in the quest for more efficient energy sources. Another recent application is a virus-based lithium battery (71) that shows performance comparable with all inorganic materials, but involves environmentally benign processes. For other examples demonstrating the use of biological materials to position fluorophores near metal nanostructures with the goal of producing more intense and stable fluorescence, we direct the reader to a recent excellent review (72).

CONCLUSION

Near-field optics, enhancement of the electromagnetic field close to metal surfaces, and surface plasmon resonances are physical phenomena often invoked in relation to their promise for building better, faster, and more sensitive sensors of biological transformations or for enabling microscopes that breach the diffraction limit and probe subcellular processes in living microorganisms. Instead of emphasizing the many ways in which biology can gain from instrumentation developed around these physical phenomena, this review highlights examples in which the trend "physical to biological" is reversed. In this sense, it is an attempt to argue that biology can advance toward the realization of materials that are useful in testing physical theories that describe materials that go beyond the conventional. By summarizing the features and advances in the field of metallodielectric materials in the first part, and some of the notable achievements in bio-enabled synthesis of 3D structures in the second part, we hope to highlight the rich, unexplored opportunities that lie at the confluence between physical and biological sciences.

DISCLOSURE STATEMENT

The authors are not aware of any affiliations, memberships, funding, or financial holdings that might be perceived as affecting the objectivity of this review.

ACKNOWLEDGMENTS

We gratefully acknowledge partial support from the National Science Foundation (grants 0832651 and 0708590) and the National Institutes of Health (grant GM081029).

LITERATURE CITED

1. Smith DR, Pendry JB, Wiltshire MCK. 2004. Metamaterials and negative refractive index. *Science* 305:788–92
2. Smith DR, Pendry JB. 2006. Homogenization of metamaterials by field averaging. *J. Opt. Soc. Am. B* 23:391–403
3. Liu ZY, Zhang XX, Mao YW, Zhu YY, Yang ZY, et al. 2000. Locally resonant sonic materials. *Science* 289:1734–36
4. Zhou X, Hu G. 2009. Analytic model of elastic metamaterials with local resonances. *Phys. Rev. B* 79:195109
5. Pendry JB, Smith DR. 2004. Reversing light with negative refraction. *Phys. Today* 57:37–43
6. Povinelli ML, Johnson SG, Joannopoulos JD, Pendry JB. 2003. Toward photonic-crystal metamaterials: creating magnetic emitters in photonic crystals. *Appl. Phys. Lett.* 82:1069–71
7. Shalaev VM. 2007. Optical negative-index metamaterials. *Nat. Photonics* 1:41–48

8. Le F, Brandl DW, Urzhumov YA, Wang H, Kundu J, et al. 2008. Metallic nanoparticle arrays: a common substrate for both surface-enhanced Raman scattering and surface-enhanced infrared absorption. *ACS Nano* 2:707–18
9. Narimanov EE, Shalaev VM. 2007. Optics: beyond diffraction. *Nature* 447:266–67
10. Caloz C. 2009. Perspectives on EM metamaterials. *Mater. Today* 12:12–20
11. Antonoyiannakis MI, Pendry JB. 1999. Electromagnetic forces in photonic crystals. *Phys. Rev. B* 60:2363–74
12. Liz-Marzan LM. 2006. Tailoring surface plasmons through the morphology and assembly of metal nanoparticles. *Langmuir* 22:32–41
13. Anker JN, Hall WP, Lyandres O, Shah NC, Zhao J, Van Duyne RP. 2008. Biosensing with plasmonic nanosensors. *Nat. Mater.* 7:442–53
14. Maier S. 2007. *Plasmonics: Fundamentals and Applications*. New York: Springer-Verlag. 223 pp.
15. Myroshnychenko V, Rodriguez-Fernandez J, Pastoriza-Santos I, Funston AM, Novo C, et al. 2008. Modelling the optical response of gold nanoparticles. *Chem. Soc. Rev.* 37:1792–805
16. Kreibig U, Vollmer M. 1995. *Optical Properties of Metal Clusters*. Heidelberg: Springer-Verlag. 532 pp.
17. Romero I, Aizpurua J, Bryant GW, Garcia de Abajo FJ. 2006. Plasmons in nearly touching metallic nanoparticles: singular response in the limit of touching dimers. *Opt. Express* 14:9988–99
18. Nordlander P, Oubre C, Prodan E, Li K, Stockman MI. 2004. Plasmon hybridizaton in nanoparticle dimers. *Nano Lett.* 4:899–903
19. Xiao JJ, Huang JP, Yu KW. 2005. Optical response of strongly coupled metal nanoparticles in dimer arrays. *Phys. Rev. B* 71:045404
20. Michaels AM, Jiang J, Brus L. 2000. Ag nanocrystal junctions as the site for surface-enhanced Raman scattering of single Rhodamine 6G molecules. *J. Phys. Chem. B* 104:11965–71
21. Yannopapas V, Modinos A, Stefanou N. 1999. Optical properties of metallodielectric photonic crystals. *Phys. Rev. B* 60:5359–65
22. Riikonen S, Romero I, Garcia de Abajo FJ. 2005. Plasmon tunability in metallodielectric metamaterials. *Phys. Rev. B* 71:235104
23. Yannopapas V. 2006. Effective-medium description of disordered photonic alloys. *J. Opt. Soc. Am. B* 23:1414–19
24. Anger P, Bharadwaj P, Novotny L. 2006. Enhancement and quenching of single-molecule fluorescence. *Phys. Rev. Lett.* 96:113002
25. Dulkeith E, Morteani AC, Niedereichholz T, Klar TA, Feldmann J, et al. 2002. Fluorescence quenching of dye molecules near gold nanoparticles: radiative and nonradiative effects. *Phys. Rev. Lett.* 89:203002
26. Ringler M, Schwemer A, Wunderlich M, Nichtl A, Kuerzinger K, et al. 2008. Shaping emission spectra of fluorescent molecules with single plasmonic nanoresonators. *Phys. Rev. Lett.* 100:203002
27. Tao AR, Ceperley DP, Sinsermsuksakul P, Neureuther AR, Yang P. 2008. Self-organized silver nanoparticles for three-dimensional plasmonic crystals. *Nano Lett.* 8:4033–38
28. Makinson REB, Roberts AP. 1960. Zone theory of liquids. *Aust. J. Phys.* 13:437–45
29. Landau D, Lifshitz M. 1960. *Electrodynamics of Continuous Media*. Burlington: Elsevier Butterworth-Heinemann
30. He Y, Ye T, Su M, Zhang C, Ribbe AE, et al. 2008. Hierarchical self-assembly of DNA into symmetric supramolecular polyhedra. *Nature* 452:198–201
31. Seeman NC. 2007. An overview of structural DNA nanotechnology. *Mol. Biotechnol.* 37:246–57
32. Mirkin CA, Letsinger RL, Mucic RC, Storhoff JJ. 1996. A DNA-based method for rationally assembling nanoparticles into macroscopic materials. *Nature* 382:607–9
33. Alivisatos AP, Johnsson KP, Peng XG, Wilson TE, Loweth CJ, et al. 1996. Organization of 'nanocrystal molecules' using DNA. *Nature* 382:609–11
34. Nykypanchuk D, Maye MM, Van Der Lelie D, Gang O. 2007. DNA-based approach for interparticle interaction control. *Langmuir* 23:6305–14
35. Chen JH, Seeman NC. 1991. Synthesis from DNA of a molecule with the connectivity of a cube. *Nature* 350:631–33
36. Goodman RP, Heilemann M, Doose S, Erben CM, Kapanidis AN, Turberfield AJ. 2008. Reconfigurable, braced, three-dimensional DNA nanostructures. *Nat. Nanotechnol.* 3:93–96

37. Goodman RP, Schaap IAT, Tardin CF, Erben CM, Berry RM, et al. 2005. Rapid chiral assembly of rigid DNA building blocks for molecular nanofabrication. *Science* 310:1661–65
38. Deleted in proof
39. Zhang YW, Seeman NC. 1994. Construction of a DNA-truncated octahedron. *J. Am. Chem. Soc.* 116:1661–69
40. Andersen FF, Knudsen B, Oliveira CLP, Frohlich RF, Kruger D, et al. 2008. Assembly and structural analysis of a covalently closed nano-scale DNA cage. *Nucleic Acids Res.* 36:1113–19
41. Zimmermann J, Cebulla MRJ, Monninghoff S, von Kiedrowski G. 2008. Self-assembly of a DNA dodecahedron from 20 trisoligonucleotides with C-3h linkers. *Angew. Chem. Int. Ed. Engl.* 47:3626–30
42. Yu H, Tao Y, Min S, Chuan Z, Ribbe AE, et al. 2008. Hierarchical self-assembly of DNA into symmetric supramolecular polyhedra. *Nature* 452:198–201
43. Aizenberg J, Weaver JC, Thanawala MS, Sundar VC, Morse DE, Fratzl P. 2005. Skeleton of *Euplectella sp.*: structural hierarchy from the nanoscale to the macroscale. *Science* 309:275–78
44. Caspar DLD, Klug A. 1962. Physical principles in construction of regular viruses. *Cold Spring Harbor Symp. Quant. Biol.* 27:1–24
45. Zandi R, Reguera D, Bruinsma RF, Gelbart WM, Rudnick J. 2004. Origin of icosahedral symmetry in viruses. *Proc. Natl. Acad. Sci. USA* 101:15556–60
46. Lewis JD, Destito G, Zijlstra A, Gonzalez MJ, Quigley JP, et al. 2006. Viral nanoparticles as tools for intravital vascular imaging. *Nat. Med.* 12:354–60
47. Steinmetz NF, Manchester M. 2009. PEGylated viral nanoparticles for biomedicine: the impact of PEG chain length on VNP cell interactions in vitro and ex vivo. *Biomacromolecules* 10:784–92
48. Douglas T, Young M. 2006. Viruses: making friends with old foes. *Science* 312:873–75
49. Uchida M, Klem MT, Allen M, Suci P, Flenniken M, et al. 2007. Biological containers: protein cages as multifunctional nanoplatforms. *Adv. Mater.* 19:1025–42
50. Sun J, DuFort C, Daniel M, Murali A, Chen C, et al. 2007. Core-controlled polymorphism in virus-like particles. *Proc. Natl. Acad. Sci. USA* 104:1354–59
51. Xiao C, Kuznetsov YG, Sun S, Hafenstein SL, Kostyuchenko VA, et al. 2009. Structural studies of the giant mimivirus. *PLoS Biol.* 7:958–66
52. Wang Q, Lin TW, Tang L, Johnson JE, Finn MG. 2002. Icosahedral virus particles as addressable nanoscale building blocks. *Angew. Chem. Int. Ed. Engl.* 41:459–62
53. Wang Q, Lin TW, Johnson JE, Finn MG. 2002. Natural supramolecular building blocks: cysteine-added mutants of cowpea mosaic virus. *Chem. Biol.* 9:813–19
54. Blum AS, Soto CM, Wilson CD, Cole JD, Kim M, et al. 2004. Cowpea mosaic virus as a scaffold for 3-D patterning of gold nanoparticles. *Nano Lett.* 4:867–70
55. Steinmetz NF, Lomonossoff GP, Evans DJ. 2006. Decoration of cowpea mosaic virus with multiple, redox-active, organometallic complexes. *Small* 2:530–33
56. Collier CP, Vossmeyer T, Heath JR. 1998. Nanocrystal superlattices. *Annu. Rev. Phys. Chem.* 49:371–404
57. Zhang HF, Hussain I, Brust M, Butler MF, Rannard SP, Cooper AI. 2005. Aligned two- and three-dimensional structures by directional freezing of polymers and nanoparticles. *Nat. Mater.* 4:787–93
58. Zheng JW, Constantinou PE, Micheel C, Alivisatos AP, Kiehl RA, Seeman NC. 2006. Two-dimensional nanoparticle arrays show the organizational power of robust DNA motifs. *Nano Lett.* 6:1502–4
59. Dixit SK, Goicochea NL, Daniel MC, Murali A, Bronstein L, et al. 2006. Quantum dot encapsulation in viral capsids. *Nano Lett.* 6:1993–99
60. Huang XL, Bronstein LM, Retrum J, Dufort C, Tsvetkova I, et al. 2007. Self-assembled virus-like particles with magnetic cores. *Nano Lett.* 7:2407–16
61. Sun J, DuFort C, Daniel MC, Murali A, Chen C, et al. 2007. Core-controlled polymorphism in virus-like particles. *Proc. Natl. Acad. Sci. USA* 104:1354–59
62. Klem MT, Young M, Douglas T. 2008. Biomimetic synthesis of β-TiO_2 inside a viral capsid. *J. Mater. Chem.* 18:3821–23
63. Uchida M, Klem MT, Allen M, Suci P, Flenniken M, et al. 2007. Biological containers: protein cages as multifunctional nanoplatforms. *Adv. Mater.* 19:1025–42
64. Chen C, Daniel MC, Quinkert ZT, De M, Stein B, et al. 2006. Nanoparticle-templated assembly of viral protein cages. *Nano Lett.* 6:611–15

65. Manchester M, Steinmetz NF, eds. 2009. *Viruses and Nanotechnology*. Berlin: Springer. 147 pp.
66. Kuznetsov YG, Makino DL, Malkin AJ, McPherson A. 2005. The incorporation of large impurities into virus crystals. *Acta Crystallogr. D* 61:720–23
67. Prodan E, Radloff C, Halas NJ, Nordlander P. 2003. A hybridization model for the plasmon response of complex nanostructures. *Science* 302:419–22
68. Aniagyei SE, DuFort C, Kao CC, Dragnea B. 2008. Self-assembly approaches to nanomaterial encapsulation in viral protein cages. *J. Mater. Chem.* 18:3763–74
69. Miller RA, Presley AD, Francis MB. 2007. Self-assembling light-harvesting systems from synthetically modified tobacco mosaic virus coat proteins. *J. Am. Chem. Soc.* 129:3104–9
70. Ma YZ, Miller RA, Fleming GR, Francis MB. 2008. Energy transfer dynamics in light-harvesting assemblies templated by the tobacco mosaic virus coat protein. *J. Phys. Chem. B* 112:6887–92
71. Lee YJ, Yi H, Kim WJ, Kang K, Yun DS, et al. 2009. Fabricating genetically engineered high-power lithium-ion batteries using multiple virus genes. *Science* 324:1051–55
72. Chen Y, Munechika K, Ginger DS. 2008. Bioenabled nanophotonics. *MRS Bull.* 33:536–42

Annual Review of
Physical Chemistry
Volume 61, 2010

Contents

Indexes

Errata

An online log of corrections to *Annual Review of Physical Chemistry* articles may be found at http://physchem.annualreviews.org/errata.shtml